PERGAMON

International Journal of Solids and Structures 39 (2002) 2517–2532

INTERNATIONAL JOURNAL OF SOLIDS and STRUCTURES

www.elsevier.com/locate/ijsolstr

Modeling the effects of hole distribution in perforated aluminum sheets I: representative unit cells

S. Jia [1], G.F. Raiser [2], G.L. Povirk [*,3]

Department of Mechanical Engineering, Yale University, New Haven, CT 06520, USA

Received 19 May 2001; received in revised form 14 January 2002

Abstract

A method is presented that incorporates microstructural information into a model of the mechanical behavior of two-phase composite materials. The approach is to determine periodic microstructures that are statistically similar to the actual microstructure of the material under consideration. The utility of this method is that computationally tractable finite element simulations can then be carried out on representative unit cells that are directly obtained from microstructural observations. To illustrate this method, mechanical tests are performed on perforated aluminum sheets with various microstructures, and the results are compared to finite element simulations of selected representative unit cells. The simulations agree with the trends observed in the experiments, including measurements of the overall strength and ductility of the sheets. Advantages and limitations of the approach used here are discussed. © 2002 Published by Elsevier Science Ltd.

Keywords: Composite; Microstructure; Spatial distribution; Unit cell; Finite element; Macroscopic behavior; Mechanical properties; Strength; Ductility

1. Introduction

Materials with two distinct phases represent a broad class of materials, including dispersion-strengthened alloys, mechanically alloyed materials, spheroidized steels, and metal- and ceramic-matrix composites. Incomplete densification during processing, creep cavitation, or void nucleation during ductile fracture can cause even nominally homogeneous materials to contain a significant fraction of voids. These voids can also be thought of as secondary phase. The microstructure of a two-phase material can in turn have a profound effect on the mechanical properties of the material, particularly on the initiation and evolution of damage. For example, research by Lewandowski et al. (1989) on aluminum–silicon carbide composites has shown

* Corresponding author. Address: 21 Chestnut Lane, 12309 Niskayuna, NY, USA. Tel.: +1-518-395-6709.
E-mail address: glpovirk@earthlink.net (G.L. Povirk).
[1] Present address: Structural Research and Analysis Corp., Los Angeles, CA 90025, USA.
[2] Present address: Intel Corp., Chandler, Arizona, USA.
[3] Present address: Knolls Atomic Power Laboratory, Schenectady, NY 12309, USA.

0020-7683/02/$ - see front matter © 2002 Published by Elsevier Science Ltd.
PII: S0020-7683(02)00115-4

that fracture usually initiates at large particles, inclusions, and regions of clustered silicon carbide particles. They also observed that damage accumulation ahead of a macroscopic crack tends to occur in regions where reinforcements are clustered together.

Many investigators have studied two-phase materials by idealizing the composite microstructure as having a simple periodic structure, with one or two reinforcing particles (or voids) within each unit cell. With this assumption, estimates of the macroscopic response of the material can be obtained by solving an appropriate boundary value problem formulated on a representative unit cell. This approach has been used to estimate the flow behavior of metal-matrix composites (Bao et al., 1991; Christman et al., 1989) and of porous metals (Koplik and Needleman, 1988). Moreover, simple unit cell models have been used to study the damage mechanisms in composite materials, such as interfacial debonding (Needleman, 1987), particle cracking (Finot et al., 1994), and ductile failure in the matrix (Llorca et al., 1991). While these analyses have provided important insights into deformation and damage initiation in these materials, they also possess significant limitations as well. One important limitation is that the predicted behavior can be strongly affected by the choice of assumed unit cell parameters (Bao et al., 1991; Povirk et al., 1992). Furthermore, a simple unit cell with one reinforcement (or void) cannot provide a realistic portrayal of damage evolution in a composite material. For example, experiments on aluminum sheets containing randomly distributed perforations showed the pronounced effects of hole distribution on resultant mechanical behavior (Magnuson et al., 1988). Corresponding finite element calculations by Becker and Smelser (1994) showed that a simple unit cell with one hole could not adequately predict the ductility of the sheets.

More recently, investigators have begun to account for the effects of microstructure on the mechanical properties of two-phase materials. A central problem that develops, however, is the computational expense associated with incorporating large amounts of microstructural information into the model. To make the problems more tractable, researchers have used different procedures to simplify the problem. For example, Ostoja-Starzewski et al. (1994) developed a finite difference lattice model in which damage evolution is simulated by sequentially removing bonds in the model if the lattice strain exceeds a critical value. While this method is quite useful in examining the effects of material constants on the qualitative behavior of composite materials, more detailed descriptions of material behavior are required to model real composite materials. Moorthy and Ghosh (1998) have developed a model in which a composite material is divided into Voronoi cells, with each cell containing one reinforcement at most. For each Voronoi cell, a stress hybrid method is used where an equilibrated stress field (derived from an Airy stress function) is assumed within the cell and displacements are interpolated on the boundary of the cell. While the method is complex, it appears to have great potential in modeling deformation and damage within composite materials. Torquato (1998) proposed a model for statistically inhomogeneous two-phase materials consisting of inhomogeneous fully penetrable spheres that permits one to represent and evaluate certain n-point correlation functions that statistically characterize the microstructure. Ibnabdeljalil and Curtin (1997) studied the failure behavior of fiber-reinforced composites using a three-dimensional lattice Green's function model under "local load sharing" conditions (i.e., stress from broken fibers is transferred predominantly to the nearby unbroken fibers). Weakest-link statistics were then employed to investigate size effects and reliability.

The intent of this work is to develop alternative tools for incorporating microstructural information into models of two-phase materials. The approach considered here is to determine a periodic microstructure that is statistically similar to the actual microstructure under consideration. With a periodic microstructure so determined, a numerical analysis can be performed on a single unit cell of the periodic structure, with an associated reduction in computational cost. To test the procedures, idealized composites are constructed by perforating aluminum sheets with various complex patterns of holes and subjecting the specimens to standard uniaxial tensile tests. After corresponding periodic microstructures have been determined, finite element simulations of uniaxial tensile tests are performed on representative unit cells and the results are

compared to experimental results. This study is a continuation of an investigation by Povirk (1995), who compared the elastic behavior of complex microstructures to that of selected representative unit cells.

2. Procedures

The general procedures used in this study are outlined as follows. Six complex patterns of circles were generated and used as templates to obtain aluminum sheets with various hole distributions. The mechanical behavior of the perforated sheets was then determined experimentally by uniaxial tensile testing. Numerical models of the six complex microstructures were developed by first obtaining corresponding unit cells that have similar spatial distributions of holes; the methods used in the determination of the unit cell parameters will be discussed subsequently. Finite element meshes were then generated for each of the six unit cells, and appropriate periodic boundary conditions were implemented. The flow behavior of the aluminum matrix was characterized by isotropic, rate-dependent J_2 flow theory, with initial strain-hardening followed by eventual strain-softening. The behavior predicted by the unit cell models were then compared to the corresponding experimental results.

2.1. Generation of hole patterns

The region in which the hole patterns were generated were assumed to occupy a rectangular region of dimensions $H_1 \times H_2$ (see Fig. 1). Each pattern was arbitrarily assumed to contain 115 holes, with the hole diameter chosen such that the area fraction was 10%. The initial step was to discretize this region into an $N_1 \times N_2$ array of points, given by

$$x_{k_1} = \frac{H_1}{N_1} k_1, \quad k_1 = 0, \ldots, N_1; \qquad y_{k_1} = \frac{H_2}{N_2} k_2, \quad k_2 = 0, \ldots, N_2 \tag{1}$$

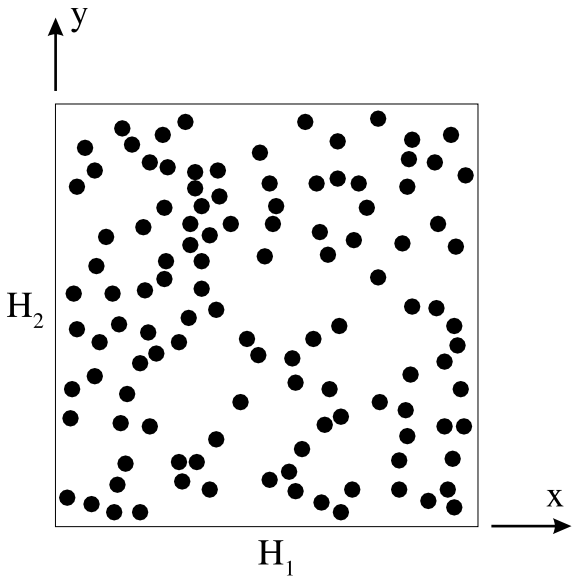

Fig. 1. Typical hole pattern used for the perforated aluminum sheets.

The hole patterns were generated by assigning, at each of the discrete points defined by Eq. (1), a number p of the form

$$p = r + \varepsilon_1 \cos\left(\frac{12\pi x}{H_1}\right) + \varepsilon_2 \cos\left(\frac{12\pi y}{H_2}\right) + \frac{\varepsilon_3}{2}\left[\sin\left(\frac{12\pi x}{H_1} - \frac{\pi}{2}\right)\sin\left(\frac{12\pi y}{H_2} - \frac{\pi}{2}\right) + 1\right] + \frac{\varepsilon_4}{2}\left[\sin\left(\frac{12\pi x}{H_1} - \frac{\pi}{2}\right)\sin\left(\frac{6\pi y}{H_2} - \frac{\pi}{2}\right) + 1\right] + \frac{\varepsilon_5}{2}\left[\sin\left(\frac{6\pi x}{H_1} - \frac{\pi}{2}\right)\sin\left(\frac{12\pi y}{H_2} - \frac{\pi}{2}\right) + 1\right] \quad (2)$$

where r represents a random number ranging from 0 to 1, and the variables ε_i are input parameters that were used to exert a measure of control over the generated patterns of holes. Circles were placed starting at the point with the maximum value of p and sequentially thereafter at points with descending values of p. Any new circle location that overlapped or touched an existing circle was rejected. Six different microstructures were generated by selecting an initial "seed" for the random number generator and choosing different values of the parameters ε_i. Templates for the aluminum sheets were generated based on the calculated hole coordinates.

2.2. Experimental procedure

Specimens were machined from 1100-H14 aluminum sheets. Each sample had a thickness of 0.81 mm, a width of 30.5 mm and a gauge length of 30.5 mm. The hole patterns were printed out on a laser printer and bonded to the aluminum tensile samples. With the template attached to the specimens, holes with a diameter of 1.016 mm were drilled in the appropriate locations. For each of the six patterns that were generated, three identical samples were prepared. After drilling, any excessive metal extending out of the holes was sanded off, and the specimens were subjected to annealing at 400 °C for 60 s. (O-temper, Baker et al., 1979).

Tensile tests were conducted on an MTS servo-hydraulic testing machine configured with a 458.20 MicroConsole using a TestLink interface. The MicroConsole was equipped with a DC controller for control and data acquisition of the loads and an AC controller for control and data acquisition of the displacement. A MTS 632.11B-20 extensometer with an attachment kit for flat sample applied was used to measure the strain of the sample. The default distance between the two knife edges of the extensometer was 25.4 mm but was modified to be 30.5 mm to match the gauge length of the sample. Another DC controller on the MicroConsole was used for control and data acquisition of the strain data from the extensometer.

One difficulty involved in the experiments was that as failure progressed, significant rotation of the specimen would often occur. This is an important problem, since the model of sheet deformation does not account for this effect. To limit this effect, we first applied a small tensile load to align the sample. Once the specimen was aligned, we then tightened two adjustable "stops" on each side of specimen to limit the rotation of the specimen during testing. The extensometer was then attached to the sample, and a constant velocity of 0.04 mm/s was prescribed to the lower grip. The load, displacement and strain (actually the distance between the two knife edges of the extensometer) was output to a computer through a LAB-PC data acquisition expansion board. A LabVIEW (1996) program was created to process these data and output the engineering stress and strain of the sample. Each sample was pulled to complete failure.

2.3. Selection of unit cell parameters

The first step in the selection of unit cell parameters is to represent a complex pattern of holes by a discrete indicator function

$$g^{c}(x_{k_1}, y_{k_2}) = \begin{cases} 0 & \text{for phase 1} \\ 1 & \text{for phase 2} \end{cases} \tag{3}$$

where phase 1 and phase 2 represents the aluminum matrix and the holes, respectively. The corresponding unit cell that will be used for the finite element calculations is described by a similar indicator function.

The power spectral density of the complex patterns is obtained at discrete frequencies by first calculating the two-dimensional, discrete, fast Fourier transform of the indicator function, $G^{c}(f_x^{n_1}, f_y^{n_2})$

$$G^{c}(f_x^{n_1}, f_y^{n_2}) = \sum_{k_2=0}^{N_2-1} \sum_{k_1=0}^{N_1-1} \exp(2\pi \mathrm{i} x_{k_1} f_x^{n_1}) \exp(2\pi \mathrm{i} y_{k_2} f_y^{n_2}) g^{c}(x_{k_1}, y_{k_2}) \tag{4}$$

at frequencies given by

$$f_x^{n_1} = \frac{n_1}{H_1}, \quad n_1 = -\frac{N_1}{2}, \ldots, \frac{N_1}{2}, \qquad f_y^{n_2} = \frac{n_2}{H_2}, \quad n_2 = -\frac{N_2}{2}, \ldots, \frac{N_2}{2} \tag{5}$$

Because the indicator function is real, its Fourier transform is independent of the signs of the frequencies $f_x^{n_1}$ and $f_y^{n_2}$. The one-sided power spectral density of the complex pattern, $P^{c}(f_x^{n_1}, f_y^{n_2})$, can then be written as Press et al. (1992)

$$P^{c}(f_x^{n_1}, f_y^{n_2}) = \begin{cases} |G^{c}(f_x^{n_1}, f_y^{n_2})|^2 & \text{for } n_1, n_2 = 0 \\ 2|G^{c}(f_x^{n_1}, f_y^{n_2})|^2 & \text{for } n_1 > 0,\ n_2 = 0,\ \text{or } n_1 = 0,\ n_2 > 0 \\ 4|G^{c}(f_x^{n_1}, f_y^{n_2})|^2 & \text{for } n_1, n_2 > 0 \end{cases} \tag{6}$$

The use of the fast Fourier transform requires that both N_1 and N_2 be powers of two. In the following discussions, frequencies with indices of n_1 and n_2 will refer to those associated with the complex hole patterns.

The next step is to choose the desired number of holes for the unit cell, an initial set of dimensions h_1 and h_2 for the cell, and an initial set of hole positions. The dimensions for the cell were chosen to yield the same area fraction of holes as in the complex patterns. The indicator function for the unit cell is then written as

$$g^{p}(x, y) = \sum_{\beta=1}^{n_p} g_0(x - \phi_x^{\beta}, y - \phi_y^{\beta}) \tag{7}$$

where $g_0(x, y)$ describes the shape of the holes, ϕ_x^{β} and ϕ_y^{β} are the coordinates of hole β and n_p is the number of holes in each unit cell. For this study, each unit cell was assumed to contain 12 holes. The unit cell is discretized by an $M_1 \times M_2$ array of points so that the fast Fourier transform of the periodic structure then takes the form

$$G^{p}(f_x^{m_1}, f_y^{m_2}) = \sum_{\beta=1}^{n_p} G_0(f_x^{m_1}, f_y^{m_2}) \exp(2\pi \mathrm{i} f_x^{m_1} \phi_x^{\beta}) \exp(2\pi \mathrm{i} f_y^{m_2} \phi_y^{\beta}) \tag{8}$$

at frequencies given by

$$f_x^{m_1} = \frac{m_1}{h_1}, \quad m_1 = -\frac{M_1}{2}, \ldots, \frac{M_1}{2}, \qquad f_y^{m_2} = \frac{m_2}{h_2}, \quad m_2 = -\frac{M_2}{2}, \ldots, \frac{M_2}{2} \tag{9}$$

and where $G_0(f_x^{m_1}, f_y^{m_2})$ represents the fast Fourier transform of $g_0(x, y)$. The corresponding power spectral density can be obtained by Eq. (6). Frequencies with indices of m_1 and m_2 will always refer to those associated with the unit cell.

Note that the discrete power spectral densities of the complex and periodic structures are, in general, obtained at different frequencies. Furthermore, assuming that the dimensions of the unit cell are smaller

than that of the random structure, the frequencies associated with the periodic structure will be spaced at larger intervals in comparison to the complex structure. Therefore, to directly compare the spectral density of each structure, the power spectral density of the complex structure has to be "rebinned" to match the frequencies of the periodic structure. For a frequency bin defined by

$$\frac{f_x^{m_1-1}+f_x^{m_1}}{2}<f_x<\frac{f_x^{m_1}+f_x^{m_1+1}}{2},\qquad \frac{f_y^{m_2-1}+f_y^{m_2}}{2}<f_y<\frac{f_y^{m_2}+f_y^{m_2+1}}{2} \tag{10}$$

the rebinned power spectral density of the complex microstructure $\hat{P}^{c}(f_x^{m_1},f_y^{m_2})$ is written as

$$\hat{P}^{c}(f_x^{m_1},f_y^{m_2})=\sum_{n_2=n_2^i}^{n_2^f}\sum_{n_1=n_1^i}^{n_1^f} w(n_1,n_2)P^{c}(f_x^{n_1},f_y^{n_2}) \tag{11}$$

where $n_1^i\leqslant n_1\leqslant n_1^f$ and $n_2^i\leqslant n_2\leqslant n_2^f$ are the range of indices whose frequency bins are within the intervals given in (10). Similarly, $w(n_1,n_2)$ represents the percentage of the frequency bin of $P^{c}(f_x^{n_1},f_y^{n_2})$ located in the intervals in (10).

For a given set of unit cell dimensions, the hole positions are found by minimizing the function

$$\chi^2=\sum_{m_2=0}^{M_2/2}\sum_{m_1=0}^{M_1/2}\left[\frac{\hat{P}^{c}(f_x^{m_1},f_y^{m_2})-(A^c/A^p)P^{p}(f_x^{m_1},f_y^{m_2})}{\hat{P}^{c}(f_x^{m_1},f_y^{m_2})}\right]^2+\Phi(\phi_x^1,\ldots,\phi_x^{np},\phi_y^1,\ldots,\phi_y^{np}) \tag{12}$$

where A^c and A^p are the areas of the entire structure and the unit cell respectively. The function Φ becomes large when holes are either in contact or very close to one another, thereby providing an artificial penalty for solutions that are inconsistent with the form of the indicator function given in (7). Conversely, when all the holes are isolated from one another, Φ becomes identically zero. The specific form of the function Φ does not significantly affect the results.

Finding the absolute minimum of χ^2 for a given set of cell dimensions was complicated by the fact that the residual χ^2 typically had many local minima. Hole positions were found by initially considering the summation shown in Eq. (12) truncated to include only a few of the lowest frequencies, and minimizing this function. Higher frequency terms were then added in the summation, and the function was again minimized. This process was repeated until all of the terms in the summation were included. Each minimization was carried out by use of the conjugate gradient method (Press et al., 1992). Several initial guesses of the hole positions were required for each set of unit cell dimensions to be assured that a reasonable correlation between the spectral densities of each microstructure was obtained. With the current state of development of the numerical procedures, convergence to the absolute minimum of χ^2 was not guaranteed. An incremental search was performed over all realistic unit cell dimensions by continually adjusting the aspect ratio h_2/h_1. The most representative unit cell had dimensions and hole positions corresponding to the smallest value of χ^2 obtained by the procedures.

The motivation for using the power spectral density to compare the complex and periodic hole patterns is that it can be thought of as a probability density function in the frequency domain Parzen (1962). Periodic hole patterns with similar spectral densities to that of the actual perforated sheets should therefore have a comparable hole distributions, and presumably, similar mechanical behavior as well. A more intuitive way of thinking about the power spectral density is that it can be loosely thought of as representing the "diffraction pattern" of a two-phase material, in that the spectral density of the indicator function is mathematically very similar to the intensity distribution given by the kinematical theory of electron diffraction (Hirsch et al., 1977). For example, if the hole distribution is highly ordered, the spectral density will have very sharp peaks, much like the diffraction pattern of a single crystal. Conversely, the spectral density becomes more diffuse as the distribution of holes becomes more random.

2.4. Finite element calculations

Simulations of uniaxial tensile tests were performed based on the selected unit cells and the results were compared to the behavior of the corresponding aluminum sheets. Finite element meshes were obtained using the commercial mesh generating program HyperMesh (1997). Finite strain, plane stress, four-node quadrilateral elements were used in all of the computations. Periodic boundary conditions were prescribed for each unit cell to ensure compatibility with surrounding unit cells and continuity of tractions across cell boundaries. Denoting the displacement and force at the upper right corner node by $\mathbf{u}^p$ and $\mathbf{F}^p$ respectively, the boundary conditions were prescribed as follows. For the four corners

$$u_x(0,0) = u_x(0,h_2) = u_y(0,0) = u_y(h_1,0) = 0 \tag{13}$$

$$u_x(h_1,h_2) = u_x^p, \qquad u_y(h_1,h_2) = u_y^p \tag{14}$$

For the nodes along the edges

$$u_x(x,h_2) - u_x(x,0) = 0, \qquad u_y(x,h_2) - u_y(x,0) = u_y^p \tag{15}$$

$$u_x(h_1,y) - u_x(0,y) = u_x^p, \qquad u_y(h_1,y) - u_y(0,y) = 0 \tag{16}$$

To simulate uniaxial tension, a nominal strain rate of $\dot{\varepsilon}_{yy} = 2.8 \times 10^{-4}\ \mathrm{s}^{-1}$ was imposed in the vertical direction, and the net forces on the sides of the unit cell were assumed to vanish. These boundary conditions are imposed through the relations

$$\dot{u}_y^p = h_2\dot{\varepsilon}_{yy}, \qquad F_x^p = 0 \tag{17}$$

The nominal stress–strain behavior of the unit cell is then given by

$$\sigma_{yy} = \frac{F_y^p}{h_1}, \qquad \varepsilon_{yy} = \frac{u_y^p}{h_2} \tag{18}$$

assuming an initial unit thickness. In addition to satisfying compatible cell deformations, the boundary conditions described above also yield the necessary condition that the tractions, $\mathbf{T}$, across cell boundaries are continuous,

$$\mathbf{T}(x,0) = -\mathbf{T}(x,h_2), \qquad \mathbf{T}(0,y) = -\mathbf{T}(h_1,y) \tag{19}$$

The stress–strain behavior obtained from (18) is for the specific unit cell, not the macroscopic behavior of the entire perforated sheet. To obtain the stress–strain behavior of the entire structure, we need to account for the fact that there is only one failure path across the structure. In the unit cell model, failure is assumed to happen simultaneously in every unit cell in the periodic structure, so that multiple failure paths are assumed. To overcome this limitation, we assume a unit cell with height h_2 is surrounded by material with effective height $H_2 - h_2$ (H_2 is the height of the entire perforated sheet structure). The surrounding material behaves exactly the same as the unit cell until the load begins to drop. At that point, we assume localization occurs in the unit cell, and no further deformation occurs in the surrounding material. In actuality the surrounding material should have a slight elastic contraction, but because the elastic strains are small compared to the plastic strains, this is an acceptable approximation. In another words, assume the stress–strain behavior obtained from (18) is $\sigma = f(\varepsilon)$ and that the stress reaches a maximum $\sigma_{\max}$ when $\varepsilon = \varepsilon_{\max}$. The stress–strain behavior of the entire structure is then approximated as

$$\sigma = \begin{cases} f(\varepsilon), & \text{when } 0 \leqslant \varepsilon < \varepsilon_{\max} \\ f\left(\frac{H_2\varepsilon - (H_2 - h_2)\varepsilon_{\max}}{h_2}\right) & \text{when } \varepsilon \geqslant \varepsilon_{\max} \end{cases} \tag{20}$$

The mechanical behavior of the aluminum was modeled as elastic–viscoplastic, with a stress–strain rate relation of the form

$$\overset{\nabla}{\tau} = \mathbf{L} : (\mathbf{D} - \mathbf{D}^{\mathrm{p}}) \tag{21}$$

where $\overset{\nabla}{\tau}$ is the Jaumann rate of Kirchhoff stress, $\mathbf{L}$ is a tensor of isotropic elastic moduli, and $\mathbf{D}$ is the total rate of deformation. The plastic rate of deformation was assumed to be isotropic, power-law viscoplasticity of the form

$$\mathbf{D}^{\mathrm{p}} = \dot{\varepsilon}_0 \left(\frac{\bar{\sigma}}{g(\bar{\varepsilon})} \right)^m \frac{3\mathbf{S}}{2\bar{\sigma}} \tag{22}$$

where $\bar{\sigma}$ is the effective stress, $\bar{\varepsilon}$ is the effective plastic strain, and $\mathbf{S}$ is the deviatoric stress. The flow strength $g(\bar{\varepsilon})$ of the aluminum was assumed to be first strain hardening, and then strain softening

$$g(\bar{\varepsilon}) = \begin{cases} \sigma_y + (\sigma_{\max} - \sigma_y)\left[1 - \left(\frac{\bar{\varepsilon}-\varepsilon_1}{\varepsilon_1}\right)^2\right]^n, & \bar{\varepsilon} \leqslant \varepsilon_1 \\ \frac{1}{2}\sigma_{\max}\left\{1 + \cos\left[\pi\left(\frac{\bar{\varepsilon}-\varepsilon_1}{\varepsilon_2-\varepsilon_1}\right)\right]\right\}, & \varepsilon_1 < \bar{\varepsilon} < \varepsilon_2 \\ 0, & \bar{\varepsilon} \geqslant \varepsilon_2 \end{cases} \tag{23}$$

The above relations were chosen so that the material strain-hardens up to a plastic strain of ε_1, strain-softens at plastic strains between ε_1 and ε_2, and has a complete loss of load carrying capacity at plastic strains greater than ε_2. The initial flow strength is given by σ_y while the maximum flow strength is indicated by $\sigma_{\max}$. The Young's modulus of the aluminum was also assumed to be a function of accumulated plastic strain

$$E(\bar{\varepsilon}) = \begin{cases} E_0, & \bar{\varepsilon} \leqslant \varepsilon_1 \\ \frac{1}{2}E_0\left\{1 + \cos\left[\pi\left(\frac{\bar{\varepsilon}-\varepsilon_1}{\varepsilon_2-\varepsilon_1}\right)\right]\right\}, & \varepsilon_1 < \bar{\varepsilon} < \varepsilon_2 \\ 0, & \bar{\varepsilon} \geqslant \varepsilon_2 \end{cases} \tag{24}$$

The addition of Eq. (24) to the model accounts for the reduction in stiffness that is expected as damage accumulates in the aluminum matrix. We incorporated the constitutive law into the commercial finite element code ABAQUS (1997) through a user-supplied subroutine UMAT, using a rate–tangent integration method by Peirce et al. (1984).

2.5. Determination of material parameters

The most obvious method for the determination of material parameters would be standard uniaxial tensile tests on (unperforated) aluminum sheets. After material softening and subsequent localization of deformation, however, the mechanical behavior of the aluminum can only be indirectly inferred through further analysis. The anticipated failure mechanism in the perforated aluminum sheets is the localization of deformation between adjacent holes. For this reason, we decided to test sheets with a uniform square array of holes, and to infer the mechanical properties of the aluminum by finite element analyses of a corresponding string of unit cells. It is hoped that the parameters determined in this manner will be most appropriate for describing the softening behavior of the aluminum in the simulations using the selected representative unit cells.

More specifically, the tensile sample used to determine the material properties had a 10×10 array of 1.016 mm holes. The holes were uniformly spaced over an area with dimensions 28.5 mm $\times$ 28.5 mm to give a hole area fraction of 10%. The simulation of the experiment was performed using a string of five simple unit cells and applying the appropriate periodic boundary conditions (see Fig. 2). To induce lo-

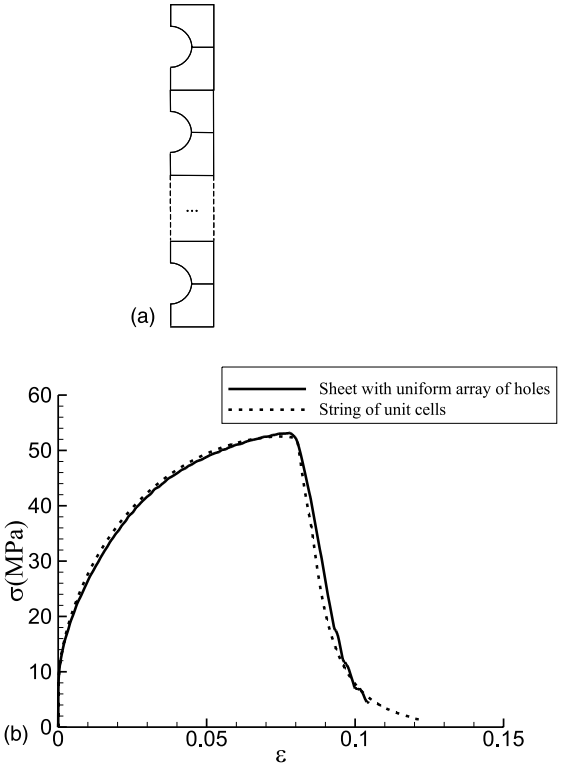

Fig. 2. Material properties obtained by comparing the behavior of aluminum sheets with a uniform array of holes to corresponding finite element simulations.

calization in only one unit cell the width of one cell in the string was made to be slightly smaller than others.

As in Becker and Smelser (1994), the stress exponent was taken to be $m = 100$, while the material parameters σ_y, $\sigma_{\max}$, ε_1, ε_2, and n were adjusted to provide a fit to the experimental data. The experimental and numerical stress–strain curves are shown in Fig. 2(b). The failure mechanism exhibited in both the experiments and the simulations was strain localization directly across the ligaments between holes. The specific material parameters used to model the aluminum matrix are shown in Table 1.

Table 1
Material properties of aluminum 1100-H14

Properties	Value
Initial Young's modulus, E_0	72000 MPa
Poisson's ratio, v	0.3
Yield strength, σ_y	9.0 MPa
Ultimate strength, $\sigma_{\max}$	81.0 MPa
Softening strain, ε_1	0.103
Failure strain, ε_2	3.5
Stress exponent, m	100
Strain rate, $\dot{\varepsilon}_0$	0.00028 s^{-1}
Strain hardening parameter, n	0.56

3. Results

The six complex patterns used in the experiments and the corresponding unit cells used in the finite element calculations are shown in Fig. 3. In each case, the periodic hole patterns appear to have a spatial distribution similar to the complex structures from which they were derived. The unit cells used for the finite element calculations are outlined in the lower left corner of the periodic structures. An example of the power spectral densities for the complex and periodic patterns is given in Fig. 4.

Photographs of the tensile specimens, both before and after testing, are shown in Fig. 5. During the early stages of loading, localized deformation occurred around all of the holes. Thin ligaments between some of the holes subsequently necked and then failed. Upon further deformation, larger ligaments between holes

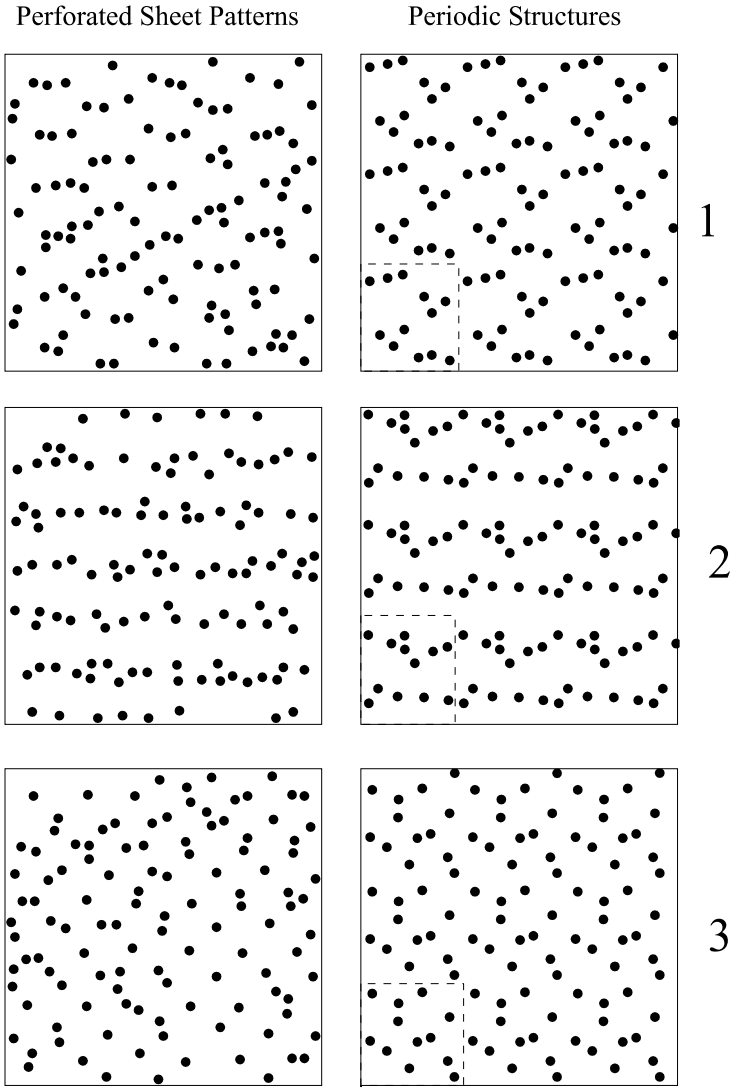

Fig. 3. Diagrams of the six microstructures used in perforated aluminum sheets (left) and their corresponding periodic structures (right). The unit cells used in finite element calculations are indicated by dashed rectangles.

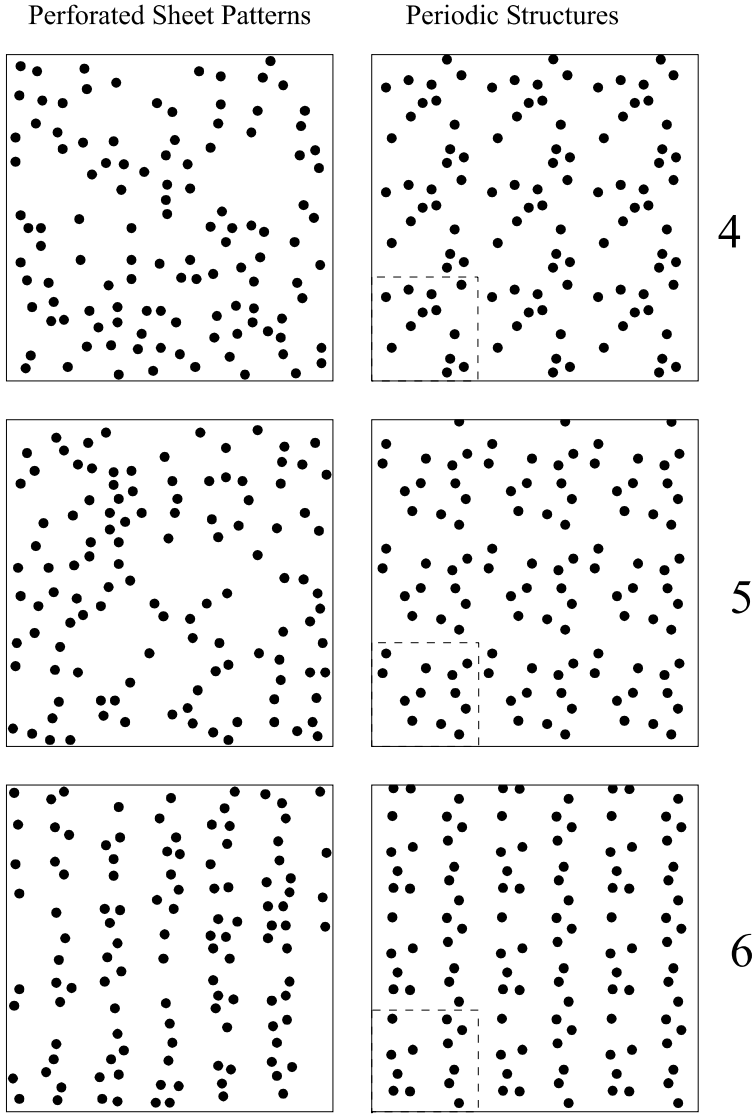

Fig. 3 (*continued*)

necked primarily along the horizontal direction. The first major drop in load corresponded to rupture of a number of these ligaments, often extending to one edge of each of the specimens.

Modeling localization and failure using the finite element method introduces a complicating factor into the analysis. Unfortunately, once localization of deformation occurs, the presence of the finite element mesh introduces an artificial length scale into the problem which in turn causes the solution to become mesh dependant. We therefore chose the mesh refinement on the representative unit cells to be about the same as the mesh density in the finite elements models that were used to obtain the material constants.

Fig. 6 compares the experimentally observed nominal stress–strain behavior to predictions based on the representative unit cells. As is evident, the prediction of stress–strain behavior is quite similar to the experimental results, exhibiting the same trends in both strength and ductility. In order to more clearly see the

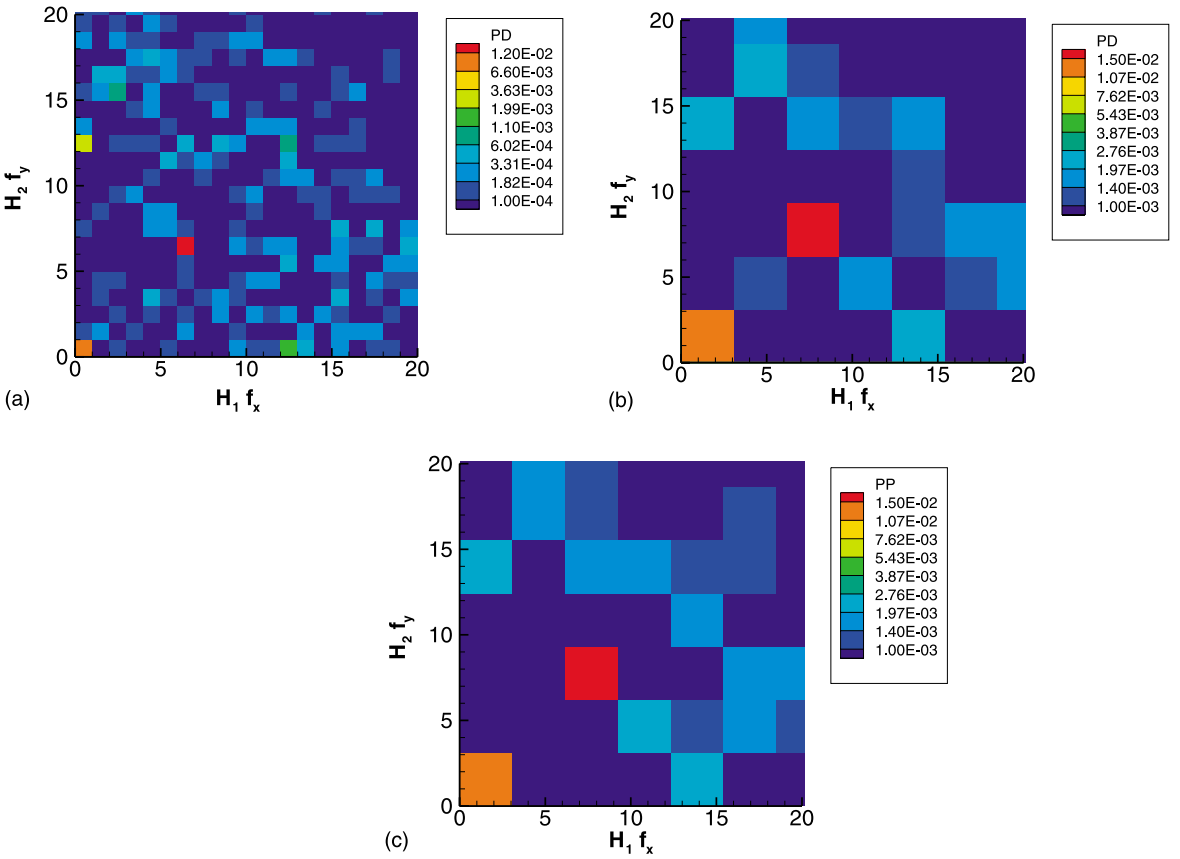

Fig. 4. Power spectral densities of (a) the original hole pattern; (b) the original hole pattern after "rebinning"; and (c) the corresponding periodic structure.

trends we also compared predicted vs experimental values of ultimate strengths in Fig. 7. The ultimate strengths from the representative unit cells has a nearly linear correlation to experimental results. The slope of the best fit line is 1.125.

Fig. 8 displays contour plots of effective plastic strain just prior to failure in each of the representative unit cells. In each case, the predicted failure path corresponds to the regions of maximum plastic strain. The effect of the periodic boundary conditions is evident, particularly for pattern #1, where the failure path meanders from the top to the bottom of the unit cell. The density of the finite element mesh used in the calculations is also clearly visible in the figures.

4. Discussion

In this investigation, idealized two-phase microstructures were constructed by perforating sheets of aluminum with random patterns of holes. They were then subjected to uniaxial tension tests so that nominal stress–strain relationships could be obtained. Each of the complex hole patterns were modeled using representative unit cells with a statistically similar distribution of holes. The unit cells were obtained by comparing the power spectral densities of the image of the original random hole pattern with that of an

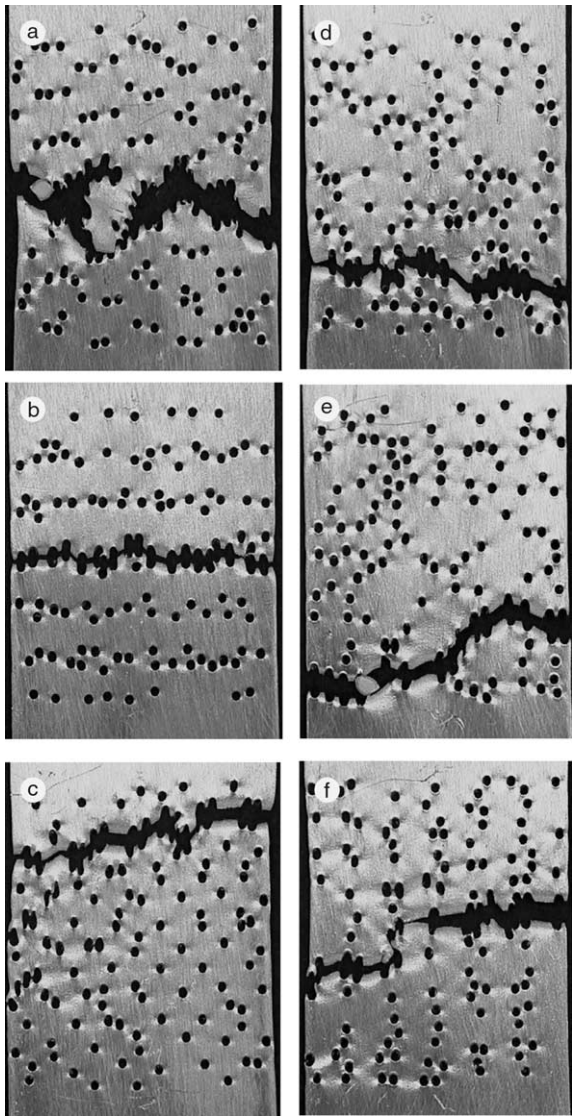

Fig. 5. Photographs of the perforated aluminum sheets after the uniaxial tensile experiments. (a)–(f) correspond to hole patterns 1 through 6, respectively.

idealized periodic pattern (Povirk, 1995). The resultant boundary value problem was solved by use of finite elements. The experimental results show the strong effect that hole distribution can have in thin sheets, which is also expected in other composite materials. The predicted nominal stress–strain curves closely match those obtained experimentally.

It is worth noting some important limitations in the methods described in this paper. One obvious limitation is that the method is restricted to two-dimensional microstructures, while composites with short fiber or particle reinforcements are clearly three-dimensional in nature. Even for three-dimensional microstructures, however, it may be possible to adequately model the composite with two-dimensional, generalized plain strain calculations. A more significant limitation in our view, however, is that the many

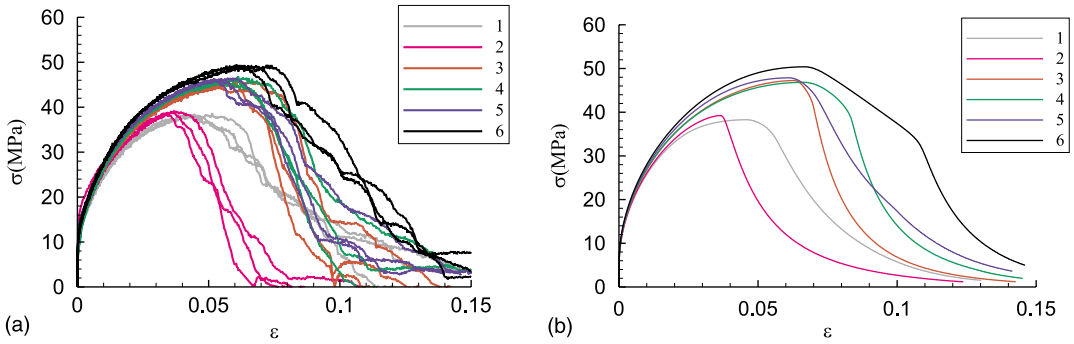

Fig. 6. Stress–strain behavior of (a) the perforated aluminum sheets; (b) the corresponding unit cell calculations. Each color represents a different hole pattern; each hole pattern was tested three times experimentally.

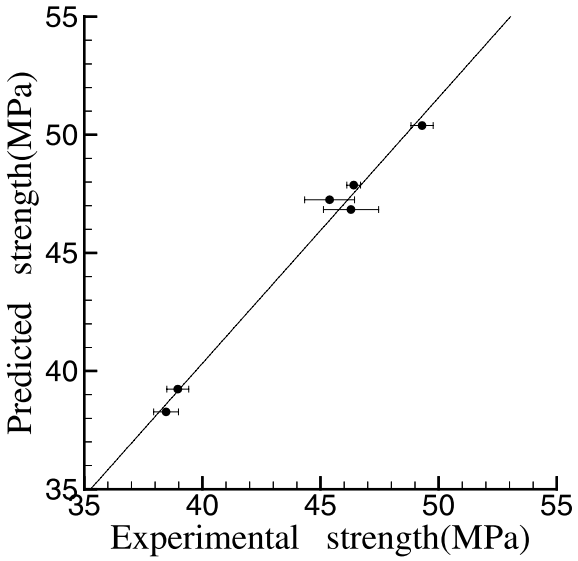

Fig. 7. Predicted ultimate strengths of the perforated aluminum sheets compared to experimental results. Horizontal bars represent the range of strength variations for the three samples of each hole pattern exhibited in the experiments.

composite microstructures (see, for example, Park et al. (1997)) have regions with large clusters of particles, and conversely, regions with little or no reinforcement. Such a microstructure would require a unit cell with much larger numbers of reinforcements than those used in the present study, which could in turn render the associated finite element calculations overly complex and computationally intractable.

The numerical methods used in this study could also be improved upon. For example, for composites that have particles of various size, morphology, and orientation, it is presently unclear as to how representative reinforcements should be selected. Moreover, there are very likely better ways to compare the spectral densities of the complex and periodic microstructures, and better ways to find the minimum of the residual function χ^2 (Eq. (12)) to ensure that the absolute minimum (and therefore the most representative unit cell) is found. Perhaps techniques used in image analysis or pattern recognition could be used to improve upon or even supplant the numerical methods used here.

Despite the limitations outlined above, however, we believe that the central ideas of this study have been validated. With our experiments, we have shown that the spatial distribution of a second phase can sig-

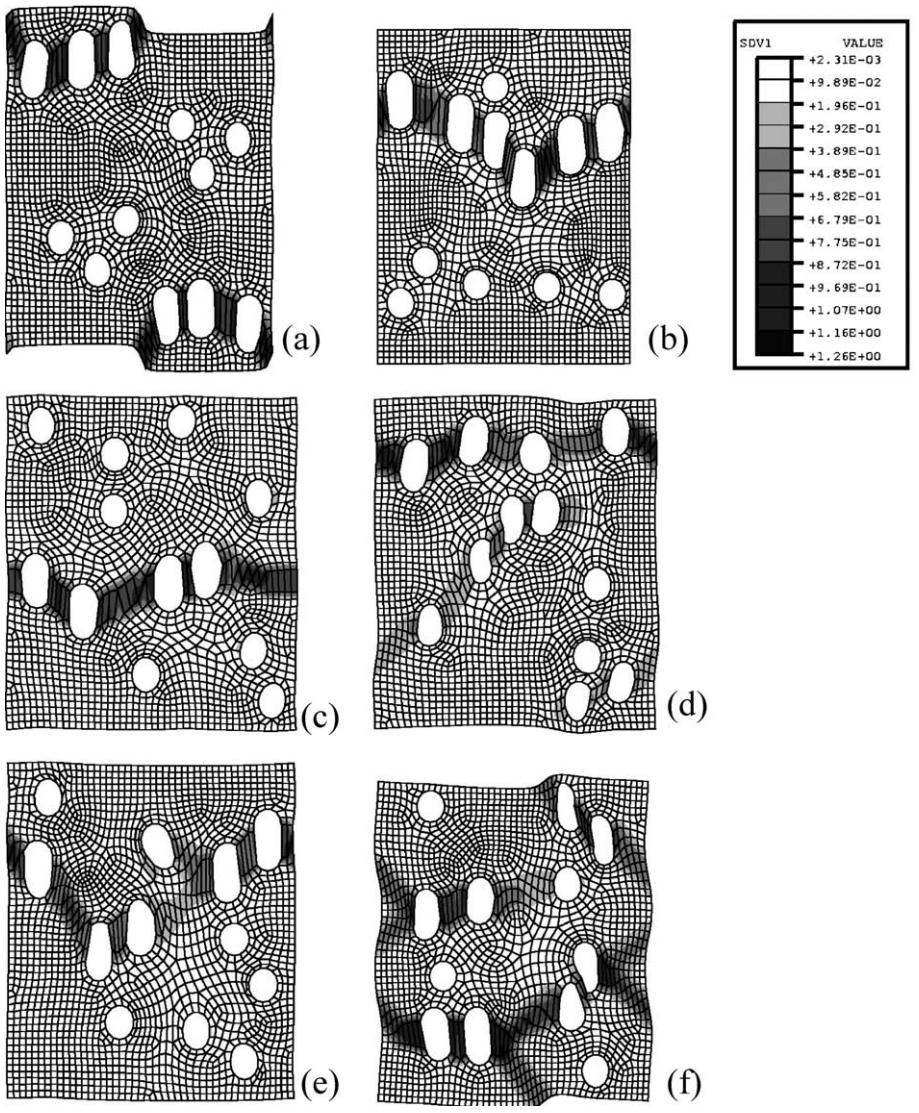

Fig. 8. Contour plots of accumulated effective plastic strain for representative unit cells. Regions of dark shading indicate elements that have completely failed. (a)–(f) correspond to hole patterns 1 through 6.

nificantly affect the mechanical behavior, particularly regarding the evolution of damage and eventual failure of the material. Using representative unit cells that have a statistically similar distribution of holes to that of the perforated aluminum sheets, we have successfully predicted the effects of hole distribution on the behavior of the sheets.

Acknowledgements

The authors are pleased to acknowledgement financial support provided by the Air Force Office of Scientific Research, contract number F49620-96-1-0198.

References

ABAQUS™ version 5.7, 1997. Hibbitt, Karlsson & Sorensen, Inc., www.hks.com.

Baker, H. et al. (Eds.), 1979. Metals Handbook, vol. 2. American Society for Metals, Metals Park OH, p. 29.

Bao, G., Hutchinson, J.W., McMeeking, R.M., 1991. Particle reinforcement of ductile matrices against plastic flow and creep. Acta Metall. Mater. 39, 1871–1882.

Becker, R., Smelser, R.E., 1994. Simulation on strain localization and fracture between holes in an aluminum sheet. J. Mech. Phys. Solids 42, 773–796.

Christman, T., Needleman, A., Suresh, S., 1989. An experimental and numerical study of deformation in metal–ceramic composites. Acta Metall. 37, 3029–3050.

Finot, M., Shen, Y.-L., Needleman, A., Suresh, S., 1994. Micromechanical modeling of reinforcement fracture in particle-reinforced metal-matrix composites. Metall. Mater. Trans. A 25, 2403–2420.

Hirsch, P.B., Howie, A., Nicholson, R.B., Pashley, D.W., Whelan, M.J., 1977. Electron Microscopy of Thin Crystals, second ed. Kreiger, Malabar, Florida.

HyperMesh™ version 2.1, 1997. Altair Computing, Inc., www.altair.com.

Ibnabdeljalil, M., Curtin, W.A., 1997. Strength and reliability of fiber-reinforced composites: localized load-sharing and associated size effects. Int. J. Solids Struct. 34 (21), 2649–2668.

Koplik, J., Needleman, A., 1988. Void growth and coalescence in porous plastic solids. Int. J. Solids Struct. v24 (n8), 835–853.

LabVIEW™ version 4.0, 1996. National Instruments Corporation, www.ni.com.

Lewandowski, J.J., Liu, C., Hunt, W.H., 1989. Effects of matrix microstructure and particle distribution on fracture of an aluminum metal matrix composite. Mater. Sci. Eng. A 107, 241–255.

Llorca, J., Needleman, A., Suresh, S., 1991. An analysis of the effects of matrix void growth on deformation and ductility in metal-ceramic composites. Acta Metall. Mater. 39, 2317–2335.

Magnuson, P.E., Dubensky, E.M., Koss, D.A., 1988. The effect of void arrays on void linking during ductile fracture. Acta Metall. 36, 1503–1509.

Moorthy, S., Ghosh, S., 1998. A Voronoi cell finite element model for particle cracking in elastic-plastic composite materials. Comput. Meth. Appl. Mech. Eng. 151, 377–400.

Needleman, A., 1987. A continuum model for void nucleation by inclusion debonding. J. Appl. Mech. 54, 525–531.

Ostoja-Starzewski, M., Sheng, P.Y., Jasiuk, I., 1994. Influence of random geometry on effective properties and damage formation in composite materials. J. Eng. Mater. Tech. 116, 384–391.

Park, J., Lenshek, D.X., Povirk, G.L., 1997. Reinforcement redistribution in Al–SiC composites under cyclic deformations. Acta Mater. 45, 1351–1364.

Parzen, E., 1962. Stochastic Processes. Holden-Day, San Francisco, California, p. 110.

Peirce, D., Shih, C.F., Needleman, A., 1984. A tangent modulus method for rate dependent solids. Comp. Struct. 18, 875–887.

Press, W.H., Teukolsky, S.A., Vetterling, W.T., Flannery, B.P., 1992. Numerical Recipes in Fortran. Cambridge University Press, Cambridge, UK.

Povirk, G.L., 1995. Incorporation of microstructural information into models of two-phase materials. Acta Metall. Mater. 43, 3199–3206.

Povirk, G.L., Stout, M.G., Bourke, M., Goldstone, J., Lawson, A.C., Lovato, M., MacEwen, S.R., Nutt, S.R., Needleman, A., 1992. Thermally and mechanically induced residual strains in Al-SiC composites. Acta Metall. Mater. 40, 2391–2412.

Torquato, S., 1998. Morphology and effective properties of disordered heterogeneous media. Int. J. Solids Struct. 35 (19), 2385–2406.